Lab on a Chip

Devices and applications at the micro- and nanoscale

Accepted Manuscript

This article can be cited before page numbers have been issued, to do this please use: J. Gai, R. Nosrati and A. Neild, *Lab Chip*, 2020, DOI: 10.1039/D0LC00457J.

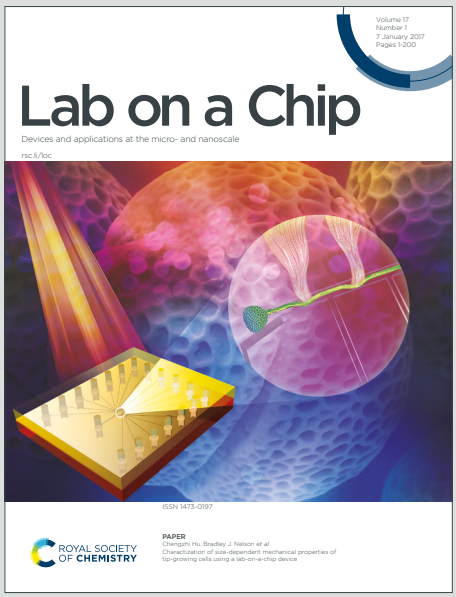

ROYAL SOCIETY OF CHEMISTRY

rsc.li/loc

High DNA integrity sperm selection using surface acoustic waves

Junyang Gai, Reza Nosrati*, Adrian Neild*

Department of Mechanical and Aerospace Engineering, Monash University, Clayton, Victoria 3800, Australia

* Corresponding authors:
Department of Mechanical and Aerospace Engineering, Monash University, Clayton, Victoria 3800, Australia
Emails: Reza.Nosrati@monash.edu (R.N.); Adrian.Neild@monash.edu (A.N.)
Phone numbers: +61 3 990 53627; +61 3 990 54655

Abstract

Male infertility is a global reproductive issue, several clinical approaches have been developed to tackle it, but their effectiveness is limited by the labour-intensive and time-consuming sperm selection procedures used. Here, we present an automated, acoustic based continuous-flow method capable of selecting high quality sperm with considerably improved motility and DNA integrity compared to the initial raw bull semen. The acoustic field translates larger sperm and guides highly motile sperm across the channel width. The result is the selection of sperm with over 50% and 60% improvement in vitality and progressive motility and more than 38% improvement in DNA integrity, respectively, while providing a clinically relevant volume and selected sperm number for the performance of In Vitro Fertilisation (IVF) and intracytoplasmic sperm injection (ICSI) by selecting over 60,000 sperm in under an hour.

Introduction

Infertility is a significant global health issue that affects ~70 million couples worldwide[1,2]. The total fertility rate has reduced significantly over the past 50 years, particularly in European Union and developed countries including Japan, the United States, Canada and Australia, with one out of each six couples experiencing infertility worldwide[2,3]. Male factor infertility is solely responsible for ~30% of the cases, with a combination of male and female factors contributing to 50% of the cases in total[4]. Multiple factors contribute to this rising trend of male infertility, including genetic mutations due to the modern life style, sexually transmitted and infectious diseases, and cancer[5]. Over the past 40 years, Assisted Reproductive Technologies (ART) have been developed to assist infertility[6] by specifically addressing issues arising from poor sperm quality[7].

ART includes intrauterine insemination (IUI), In Vitro Fertilization (IVF), and intracytoplasmic sperm injection (ICSI)[4]. In IUI, the method closest to the natural fertilization, a selected population of sperm is directly introduced higher into the female reproductive tract,

making the fertilisation process a shorter race for sperm[8]. IUI is a suitable treatment for males with relatively high concentration of motile sperm and females with normal and healthy fallopian tubes[8]. To increase the chance of fertilisation, IVF and ICSI have also been introduced as the more invasive methods, in which fertilization (*i.e.* fusion of sperm and egg) happens *ex vivo* to produce the embryo, and then after ~5 days of incubation to ensure blastocyst formation, the embryo is placed into the uterus[9]. IVF involves combining the egg with a drop of selected sperm *in vitro* (30 µL with ~50,000 selected sperm), while in ICSI, an individual sperm is selected and injected directly into the egg[10]. In all of these ART methods, the quality of the selected sperm is critical to the success rate of assisted reproduction and the subsequent health of the offspring[11]. Currently, ART success rate has plateaued at ~33% due to highly manual and subjective sperm selection practices in different clinics, mainly focusing on sperm motility as the selection criterion[2,12,13]. Whilst to develop an optimal selection strategy, all the established metrics of sperm quality (vitality, motility, morphology, and DNA integrity) should be considered.

Conventional sperm selection methods in clinics include the use of the swim-up technique and density gradient centrifugation, both of which select sperm based on their swimming characteristics[14]. In swim-up, motile sperm swim from a sedimented raw semen sample into a fresh layer of media while dead cell and debris remain behind[14]. In the density gradient method, motile sperm are aided by centrifugation to leave the seminal plasma (leaving dead cells and debris behind) and penetrate a discontinuous gradient of density to form a soft pellet in the last layer[15]. While both of these methods provide pre-screening only based on motility, they also suffer from other limitations such as low throughput (particularly in the case of semen samples with considerably low sperm concentrations)[14], generation of reactive oxygen species, (particularly due to centrifugation), and damage to sperm DNA[16]. Moreover, in case of ICSI, which is the most invasive but also the most successful and common clinical treatment method, the selection process is routinely followed by human intervention to manually select the sperm with the most normal morphology. This amounts to an expensive, time-consuming, and subjective process resulting in suboptimal pregnancy outcome[2,17].

Microfluidics enables fluidic environment to be precisely controlled and manipulated at submillimetre scales, offering the possibility of simplifying and improving medical and biological practices[18–20]. With respect to infertility, microfluidics has been used to develop technologies for diagnosis[21–23], for the fundamental understanding of sperm motion[24–26], and for high-quality sperm selection[27–29]. Passive and active mechanisms have been used in these

sorting platforms to select sperm based on their motility[10,11,27,30], response to flow[31,32] chemical gradient[33] and/or an applied electric field[34]. More recently In passive strategies, the microchannel geometry provides swimming pathways to select motile sperm by closely mimicking the natural *in vivo* microenvironment[10]. However, several factors have limited translation and clinical adoption of these passive microfluidic technologies, these include the complexity of their operation and lack of sufficient throughput, while other factors such as the intensive fabrication processes and structural irregularities have also limited mass production for commercialization[35]. In active mechanisms, sperm are selected based on their surface charges, ability to cross and swim against laminar flow streamlines, or response to a chemoattractant[33]. Active sorting strategies provide flexibility in operation[23] and enable a wider range of selection based criteria such as surface charge[36], but they still suffer from blockage issues for continuous operation to achieve the required throughput.

External force fields such as optical[37,38], magnetic[39–41], dielectrophoretic[42] and acoustic fields[43] have been applied in microfluidic platforms to achieve high-throughput sorting. With each of these methods featuring advantages in terms of throughput and sample properties, acoustic methods are particularly suitable for biological sorting applications as they can provide precise spatial control of living organism without damaging either the cell membrane or intercellular DNA structure when operated at low intensity[44]. Bulk acoustic wave (BAW)[45,46] and surface acoustic wave (SAW)[47,48] are the two acoustic actuation methods most commonly employed in microfluidic devices. In BAW a compressional wave is generated in the bulk of a piezoelectric ceramic which is typically bonded to the underside of the microfluidic chip. Operation is usually at a frequency that matches the resonant mode of the fluidic volume, hence a standing wave field is generated within the fluid[49]. More recently, bulk acoustic wave has been used to isolate low number of sperm cells from female DNA by Xu. et al[50]. However, in BAW, the constraint of operation at a fluid resonance limits the range of acoustic fields which can be produced, and in addition, the relatively low excitation frequency ranges (0.1-10 MHz) in BAW restricts the working power range for cell manipulation applications[51].

In SAW, the acoustic wave propagates along the surface of the piezoelectric material, after generation by a series of interdigital transducers (IDT) patterned on a piezoelectric substrate. The operating frequency in SAW actuation is chosen such that the vibration from each finger pair in the IDT constructively interferes. Most of the power is confined within one wavelength distance vertically from the substrate[52]. Compared with BAW, SAW can operate at a wider frequency range (20-150 MHz) by simply changing the arrangement of interdigital

transducers[53], while acoustic fields can be produced in arbitrary locations and orientations with respect to microfluidic channels (with no restriction to excitation of fluid mode resonances)[54]. Using the freedom in sound field design offered by SAW actuation, Collins *et al.*[55] developed a virtual deterministic lateral displacement (vDLD) method for continuous size-based separation of microparticles, in which the IDTs are orientated at an angle to the microfluidic channel, and the resulting SAW laterally displaces particles across the channel deterministically based on their size.

In this work, we utilise the principle of the vDLD approach, and apply it to the sorting of bull sperm from raw semen specimens. Whilst previously a high degree of size-based sorting accuracy was demonstrated (for example removing 6μm particles from 7μm)[55], the bull sperm sample is relatively homogenous in size, motile and non-spherical. Through studying the interaction of the surface acoustic generate sound field with the sperm cells, and the alignment of the swimming motion that this causes, we demonstrate that the sorting is mostly due to the degree of motility of the individual sperm cells. To demonstrate the performance of the device to select high-quality sperm, the quality of selected sperm from the device are evaluated in terms of concentration, vitality, motility, morphology and DNA integrity and compared with the quality of sperm in the initial raw sample.

System Principle

The principle of operation of the vDLD system[55] is that suspended cells (sperm, somatic cells and debris in the sample) are laterally displaced across the width of a microfluidic channel by a distance determined by their size. The term virtual refers to the lateral displacement occurring due to the application of a sound field rather than due to physical obstructions. Hydrodynamic focussing is used to introduce the cells into the sound field along the edge of the channel, where the laminar flow is slowest (Fig. 1a). The sound field acts oblique with respect to the flow to deflect the cells across flow streamlines. The interplay between acoustic forces and drag causes two distinct outcomes determined by the cell size that enable sorting. Firstly, the drag may be sufficient to overcome the acoustic forces meaning that the cell will travel through the forcefield along a single streamline. The second is that the acoustic forces are large enough to capture the cell in the sound field, against the drag force. In this second outcome, as the sound field is orientated at an angle to the flow, the cell is trapped in the acoustic node or antinode, and migrates across the width of the channel (Fig. 1). In doing so, the cell will enter faster

View Article Online
DOI: 10.1039/D0LC00457J

moving parts of the laminar flow field, increasing the drag forces, until drag dominates and pulls the cell out of the sound field. In addition, as a by-product of generating acoustic field, a time-averaged dielectrophoretic field also plays a role in the sorting procedure. Moreover, dielectrophoretic effects, as shown in previous research[36], can also contribute to selection sperm based on their viability. However, as was discussed for a similar set up[55], the height of chamber (h) relative to the vertical component of the standing wave in the fluid (λ_v) will decide which force is dominant in sorting and acoustic force becomes dominant when $h > 3/2\lambda_v$, which is analogous with our set up. Therefore, the device mainly relies on the applied sound field to separate sperm.

Considering the cell as a spherical particle in a standing wave field (as exists above the IDTs), the maximum acoustic radiation force, F_{aco}^{max}, is determined by volume, given by:

$$F_{aco}^{max} = -\left(\frac{\pi P^2 V_c \beta_f}{2\lambda}\right)\left(\frac{5\rho_c - 2\rho_f}{2\rho_c + \rho_f} - \frac{\beta_c}{\beta_f}\right)$$

where P is the acoustic pressure amplitude, which varies across the IDT finger pairs, , λ is the wavelength, ρ_p and ρ_c are the density of the fluid and cells, β_c and β_f are the compressibility of the cell and fluid medium, and V_c is the cell volume. Whilst Stokes drag is proportional to radius, given by

$$F_D = 6\pi r \eta v$$

where r is the particle radius (or the cell radius in our case), η is the fluid viscosity, and v is the differential velocity between particle and medium. Hence, for a smaller cell the drag will dominate and for a larger cell acoustic radiation is more significant. With the cut off between "smaller" and "larger" being determined by a balance of the applied acoustic power and the flow rate.

Whilst the physics for spherical inert particles and cells is established, in this work the objects which require sorting are non-spherical and motile (motile sperm out of non-motile and/or dead sperm, somatic cells, and debris). The structure of a sperm cell can be divided into three parts: the head, midpiece and tail. Based on the volume and density difference, each part can be expected to be subjected to different magnitude of acoustic radiation force. The bull sperm used in these experiments have a head volume of ~95 μm^3, a midpiece volume of ~19 μm^3 and a tail volume of ~9 μm^3 [56]. Since the bull sperm head has the largest portion of the total volume, acoustic radiation force exerted on the head will be much larger compared with the other parts.

For the case of dead immotile sperm, the result is that the vDLD accurately sorts based on head size, even for subtle size difference (within 1 μm) as shown in ESI† Movie. S1.

However, for a swimming sperm (both live and motile sperm), motility plays a dominant role in the sorting process. We observe that the usually random nature of the swimming motion (in bulk fluid) is rotationally aligned by the acoustic trap because of the nonlinear acoustic radiation torque experienced by non-spherical particles in an ultrasonic field[57], causing directed swimming. The result is a sort based on swimming process, as will be characterised experimentally and presented in Fig. 1.

Methodology

Device fabrication

The microfluidic device comprises a PDMS layer with patterned microchannels bonded onto a lithium niobate (LN) substrate which is patterned with IDTs. First, a single set of IDTs with 16 finger pairs were patterned on a 0.5 mm thick, double side polished 128° Y-cut, X-propagating LN substrate using E-beam thermal evaporation. The IDTs were fabricated by coating 10 nm of Titanium (adhesive layer), 250 nm of gold (anti-corrosion and conductive layer) and 5 nm of chromium (adhesive layer) on the LN substrate, followed by lift off to produce the required finger patterns. Once patterned, the LN substrate was then uniformly coated with 400 nm of SiO_2 to prevent direct contact between cells and the electrodes, and to promote adhesion to the PDMS layer. The 25 μm high microchannels were cast in PDMS (SYLGARD® 184, Dow Corning, with 1:5 mixing ratio of curing agent and polymer) using established soft lithography techniques. The 1:5 mixing ratio of curing agent and polymer was used to increase the stiffness of the PDMS device to prevent device deformation under SAW actuation and allow for clear visualization of the selection process. The silicon wafer mold was prepared using the Bosch process deep reactive ion etching (Oxford Instruments PLASMALAB100ICP380), and then a C4F8 hydrophobic layer was applied for enhancing the removal of PDMS. Once cast and removed from the mold, the PDMS layer was then bonded to the LN substrate, to complete the device geometry, using an air plasma (Harrick Plasma PDC-32G, Ithaca, NY, 1000 mTorr, 18 W).

Sperm preparation

Bull semen straws were purchased from ABS Global Australia and stored in liquid nitrogen. Before the experiment, the specimens were thawed in a 37 °C water bath for one minute and extracted from the straw using an artificial insemination syringe. Live and dead sperm in the

View Article Online
DOI: 10.1039/D0LC00457J

sample were then labelled with green and red fluorescence, respectively, using LIVE/DEAD sperm viability kit (ThermoFisher).

Buffer preparation

The base buffer solution used in this experiment consists of HEPES (4-(2-Hydroxyethyl)piperazine-1-ethanesulfonic acid) (21 mM), NaCl (117 mM), KCL (5.3 mM), $CaCl_2$ (2.3 mM), $MgSO_4$ (0.8 mM), $Na_2HPO_4 \cdot 2H_2O$ (0.8 mM), D-Glucose (5.5 mM), Phenol Red (0.03 mM), $NaHCO_3$(4 mM), Na Pyruvate (0.33 mM), and Na Lactate (21.4 mM). Additionally, 1mg/mL of PVA (Poly(vinyl alcohol)) is added to the base buffer to prevent sperm cells from sticking to the channel. The pH of the final solution was then adjusted to 7.4 using 1 M NaOH solution. The buffer was stored at 4 °C and used within two weeks.

Experimental procedure

The microfluidic device was mounted on a customized microscope stage, consisting of a 3D printed platform for stabilisation and a cooling system for maintaining the fluid temperature in the microchannel. The cooling system consisted of a Peltier cooler directly in contact with the SAW chip, a temperature sensor, and a heat sink to monitor the temperature and overcome the significant heating effect caused by SAW (especially at higher applied power). Two syringe pumps (KD Scientific Legato 210, Holliston, MA, USA) were then used to introduce the sperm sample and buffer on-chip at the flow rates of 0.2 µL/min and 1 µL/min, respectively. Using a power signal generator (BelektroniG F20 Power Saw, Freital, Germany), the standing surface acoustic field was then generated by applying a sinusoidal voltage signal at a resonant frequency of 19.3 MHz across the IDTs. The input power, measured using a power meter (Rhode & Schwarz NRP18S-25 Power sensor, Munich, Germany), and reported as the SAW actuation power. For SAW actuation power of 1W and 2W the actual power converted to SAW was estimated using S11 to be 0.836W and 1.672W, respectively. An upright fluorescence microscope (Olympus BX43, Tokyo, Japan) equipped with a 5-MP C-mount PixeLink camera (PL-B872CU, Ottawa, Canada) was used to image the selection process using a 20× magnification objective at 14 frames per second. After running the device for 50 min, samples extracted from each of the device outlets were analyzed to evaluate sperm concentration, vitality, motility, morphology and DNA integrity as compared with the initial raw sample.

Concentration and vitality analysis

View Article Online
DOI: 10.1039/D0LC00457J

To quantify sperm concentration and vitality, live and dead sperm in the sample were stained with SYBR14 and Propidium Iodide (LIVE/DEAD™ Sperm Viability Kit, ThermoFisher), respectively. Briefly, 5 µL of 50-fold diluted SYBR14 in DMSO and 5 µL of Propidium Iodide were added to 250 µL of the sperm sample, and the sample was incubated at 37 °C for 10 min to complete the staining. After the experiment, the initial raw sample and extracted cells from each of the outlets were each loaded into a haemocytometer (Paul Marienfeld Gmbh & Co. KG, Germany), and 20× magnification images were captured in bright field (total sperm concentration), green fluorescence (live sperm) and red fluorescence (dead sperm) for evaluating sperm concentration and vitality (ratio of live sperm to total sperm concentration).

Motility analysis

To quantify sperm motility, an image sequence of live sperm in the haemocytometer was recorded for at least 10 seconds and then processed using the OpenCASA plugin in ImageJ. Sperm motility parameters were calculated as curvilinear velocity (VCL), average path velocity (VAP), straight line velocity (VSL), beat cross frequency (BCF), lateral head displacement (ALH) and linearity (LIN)[18,58]. For statistical analysis, data were processed in Prism Graphpad. T test with Welch's correction was used to analyse statistical significance, and when applicable $P \leq 0.05$ was considered as significant.

Morphology analysis

Sperm morphology was assessed using Haematoxylin (Sigma-Aldrich) and Eosin (Sigma-Aldrich). A smear of sample (20µL) was prepared on a glass slide by putting another glass slide in contact with the aliquot of sample and drawing it along the edge. The smear slide was then dried in air, and sperm were fixed by applying 4% PFA (paraformaldehyde, Sigma-Aldrich) for 10 minutes. The smear slide was then stained with pre-filtered Harris Haematoxylin solution containing $C_{16}H_{14}O_6$(8.4mM),C_2H_5OH(343mM) $KAl(SO_4)_2$ (105.4mM), $NaIO_3$(2.6mM) and CH_3COOH (349.4mM) for 13 minutes to stain the nucleus, and then treated with Scott's Tap water consisting of $NaHCO_3$(42mM) and $MgSO_4$(166mM) for 1 minute. Eosin containing $C_{20}H_6Br_4Na_2O_5$ (2.9 mM) and C_2H_5OH (2.78 mM), was then applied for 5 min to stain cytoplasm. After each step, the smear slide was washed in water at least twice and then air-dried before observation. An inverted microscope (Nikon Eclipse Ts2, Tokyo, Japan) equipped with a CCD microscope camera (INFINITY3-3UR, Lumenera) was

View Article Online
DOI: 10.1039/D0LC00457J

used to capture 40x magnification images which were then processed in ImageJ to evaluate sperm morphology (head length and head width).

DNA analysis

Sperm chromatin dispersion test (SCD) was used for sperm DNA analysis, using SpermFunc ® DNAf (BRED Life Science Technology Inc, Shenzhen, China). The reagents were incubated for 20 minutes at 80 °C and 37 °C for at least 5 minutes before use, and then mixed with the sperm sample (concentration of 5-10×10^6 sperm per millilitre). 30 µL of the sample was then dispensed on a slide pre-coated with agarose and incubated at 4 °C for 5 minutes to solidify. The slide was then immersed in solution A (HCl based acid solution) for 7 minutes, solution B (lysing solution) for 25 minutes, and then washed with DI water for 5 minutes. After dehydration in increasing concentration of ethanol (70%, 90%, 100%; each for 2 minutes), the slide was air-dried, and stained with Wright's staining solution for 30 minutes. A minimum of 100 sperm per sample were then evaluated under 40x magnification using an inverted fluorescent microscope (Nikon Eclipse Ts2, Tokyo, Japan) equipped with a CCD colour camera (INFINITY3-3UR, Lumenera). Sperm with halo thickness, B, less than 1/3 of the smallest dimension of the head, A, was regarded as sperm with DNA fragmentation[59], and at least 100 sperm were evaluated to quantify the DNA fragmentation index (%DFI).

Results and Discussion

The acoustofluidic sperm selection device comprises of a PDMS microfluidic channel aligned on top of a SAW chip (Fig. 1a). Raw semen specimen was introduced on-chip at the flow rate of 0.1 µL/min from one of the inlets, while pure buffer at the flow rate of 1 µL/min (injected from the other inlet) was used to confine the main sample stream within a one third of the microchannel width. The device enabled high-throughput isolation of live motile sperm from the raw semen sample using an acoustic field applied at a 30° angle to the flow direction. Since both forces are differently correlated with the cell size, the interplay between acoustic forces, caused by the applied standing surface acoustic waves (SSAW), and viscous drag pushes the cells laterally across the microchannel based on their size (Fig. 1b). With the application of SSAW at 19.28 MHz and 1-2W, the acoustic radiation force was large enough to overcome the drag and guide the motile sperm to swim across the microchannel width, while somatic cells and other debris followed the mainstream, enabling a continuous, high-throughput, and size-dependent selective process for isolating motile sperm.

In addition to enabling a size-dependant selection process, the applied SSAW field aligns the cells and provides virtual pathways to facilitate the selection of highly motile sperm. Fig. 1c shows the distribution of dead sperm over the IDTs in the absence of flow within the device, demonstrating alignment of dead cells parallel to the IDTs under SSAW actuation at 19.28 MHz and 1 W (see ESI† Movie. S2). For cells exposed to the SSAW field, the size-dependant acoustic radiation force (acting perpendicular to the IDTs) pushed the cells from pressure antinodes located over the IDTs to pressure nodes to trap the cells in acoustic force minima in between the IDTs. The nonlinear acoustic radiation torque, as demonstrated for non-spherical particles in an ultrasonic field[57], also contributes to align the cell along these pathways and direct the swimming direction. In case of live motile sperm, this alignment provided virtual navigation pathways for sperm by suppressing their random swimming trajectories in all directions into directed trajectories parallel to the IDTs (Fig. 1d, see ESI† Movie. S3). Cho *et al.*[31] demonstrated a device to sort sperm based on their ability to cross laminar flow streamlines in a similar design. However, in that device, the selection process solely relied on sperm motility, with motile sperm at the lower level next to the wall never leaving the boundary to cross the streamlines, resulting in a relatively low throughput. Our controlled experiments in the absence of an applied acoustic field (*i.e.* absence of virtual swimming pathways to direct motile cells) also demonstrated that majority of sperm in the initial raw sample simply flow the main stream and discarded, with only 0.5% of sperm exhibiting sufficient motility to leave the main stream and swim across the channel (unguided by the acoustic field) to be retrieved from the selected cell outlet (see ESI† Fig. S1).

Fig. 1e shows a sequence of images for an individual motile sperm in response to SSAW actuation. The results demonstrate that acoustic forces transfer the cell to pressure nodes and also reorient the sperm parallel to the IDTs. While subjected to the SSAW field, the larger sperm head experiences larger acoustic forces than the sperm tail and quickly aligns with the pressure nodes (in ~0.12 s) while it takes longer for the sperm tail to align (>0.17 s). Alignment with pressure nodes and reorientation parallel to the IDTs both contribute to amplify the lateral displacement of motile sperm and facilitate the selection of highly motile sperm, as they swim along the pressure nodes.

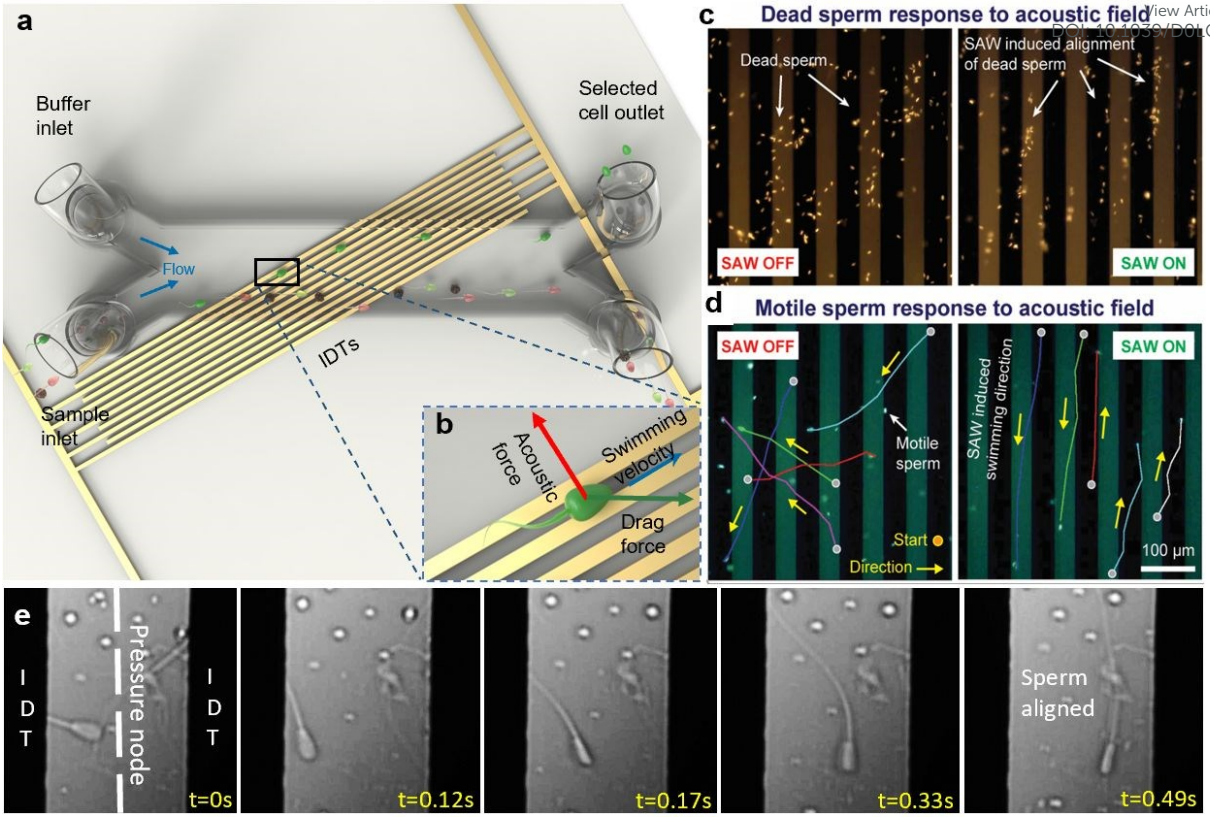

Figure 1. Acoustic-based microfluidic sperm selection device. (a) Schematic view of the device where motile and morphologically normal sperm are laterally displaced and separated from other cells and debris. (b) Acoustic forces overcome the viscous drag to transfer the sperm laterally across the microchannel width. (c) Random distribution of dead sperm over the IDTs without the application of SAW (SAW OFF, left) and alignment of the cells along the pressure nodes with the application of SAW (SAW ON, right). (d) Trajectories of randomly swimming and directed sperm in the absence (SAW OFF, left) and presence of an applied acoustic field (SAW ONN, right), respectively. (e) Reorientation and alignment of individual sperm along the pressure nodes in between the IDTs under an applied acoustic field (applied at t=0 s).

To ensure biocompatibility, sperm concentration and vitality were quantified for both the initial raw sample and cells collected from the device outlets (both outlets combined) under SSAW actuations at 0, 1, and 2 W, at 19.28 MHz (Fig. 2). The initial raw sample was mixed with the buffer with a 10:1 mixing ratio to resemble the dilution of sample in the device. As shown in Fig. 2a, sperm concentration in the initial raw sample was 7.07±5.02 million per millilitre (M/mL) and remained almost the same for samples collected from the device outlets in the absence of an applied acoustic field (0 W, cells were only exposed to shear flow) and after acoustic excitations at 1 W and 2 W (corresponding concentrations of 8.32±5.33 M/mL and 7.85±4.52 M/mL). Similarly, percentage vitality of sperm in the raw sample (33±6%) was almost identical to the percentage vitality of cells collected from the device regardless of the applied power (33±6% at 0 W, 34±2% at 1 W, and 35±2% at 2 W). The results confirm that neither the flow nor the applied acoustic fields induce cell lysis, blockage or other potential harmful effects to sperm, providing a biocompatible approach for sperm selection.

View Article Online
DOI: 10.1039/D0LC00457J

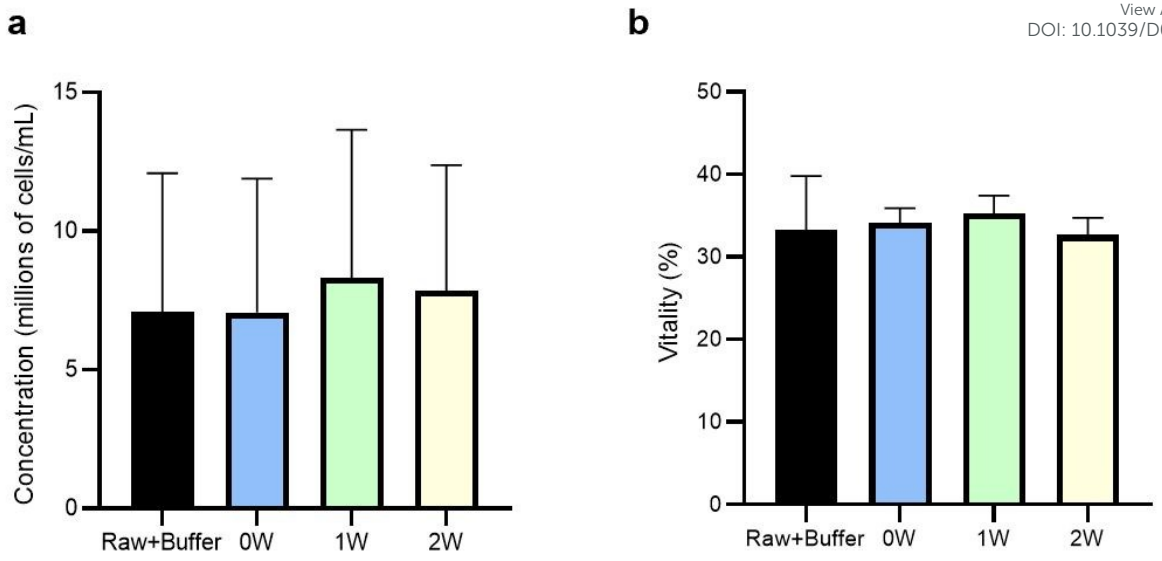

Figure 2. Biocompatibility of the acoustofluidic sperm selection approach. (a) Concentration and (b) vitality of sperm after SAW exposure at 19.28 MHz for 15 min as a function of applied power (n=3). Values are reported as mean ± s.d.

Fig. 3 shows selected sperm concentration, vitality and progressive motility in comparison with the initial raw semen sample and the discarded subpopulation of sperm that remained in the mainstream (not deflected by the SSAW field and retrieved from the discarded cell outlet). Compared with biocompatibility analysis experiments, the experiment duration was extended to 50 min in sperm selection experiments to allow for the collection of ~30 µL of sample from each of the outlets, containing enough number of sperm for subsequent quality analysis. From the initial raw sample with an average concentration of 100 M/mL, ignoring the presence of cell clusters in the cell groups, on average 2% of the total sperm population retrieved out of the raw sample with corresponding selected sperm concentration of 2.04 M/mL (with 136 M/mL and 3 M/mL as the maximum sperm concentrations in the initial raw sample and selected cells, respectively). Considering the initial raw sample concentration of ~100 M/mL and the 5µL of the raw sample processed on-chip during the 50 min device operation, the device processed ~140 sperm per second – a high-throughput for a microfluidic sperm selection technology. Despite of certain number of cell loss due to stiction and lysis, more than 60,000 sperm were collected in the 30 µL of selected sample, sufficient for the performance of droplet-based IVF (requiring ~50,000 sperm) and ICSI (requiring only one sperm)[10]. Fig. 3b shows the percentage vitality of selected sperm in comparison with the raw sample and discarded population. The selected sperm population demonstrated 50% improvement in vitality when compared with the raw sample, with corresponding vitality of 45% and 30%, respectively. The vitality of discarded cell was 37%, slightly higher than the

View Article Online
DOI: 10.1039/D0LC00457J

initial raw sample. This increase in discarded cell vitality is possibly attributed to the lysis of dead sperm with broken membranes when subjected to the acoustic force (see ESI† Movie S2). The extended experiment duration may also contribute to this phenomenon, and to the slightly lower vitality values reported in Fig. 3b for the initial raw sample compared to bio-compatibility results in Fig. 2b.

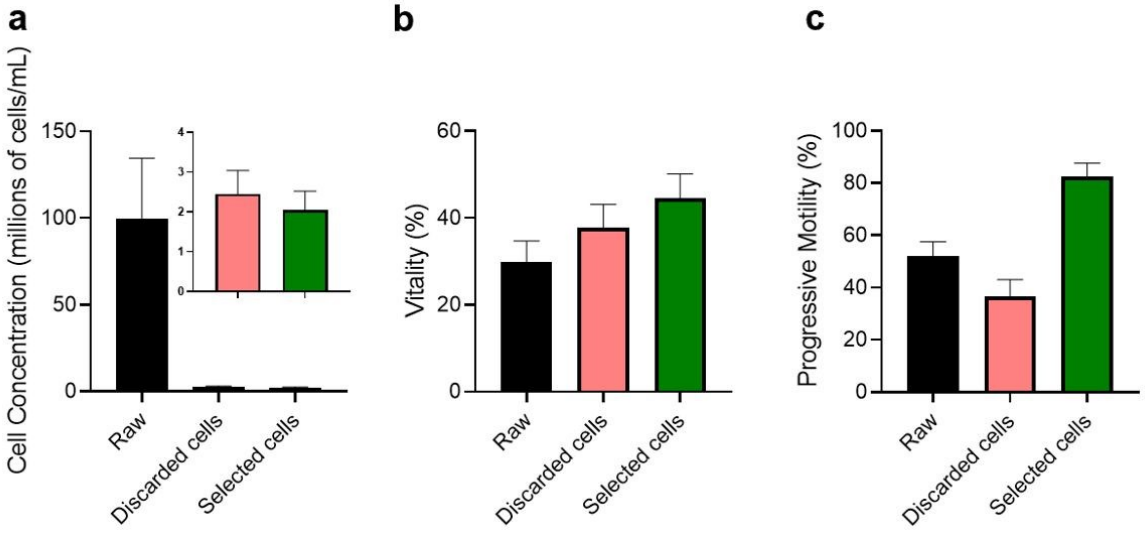

Figure 3. Sperm quality analysis. (a) Sperm concentration, (b) vitality, and (c) progressive motility for selected sperm compared with the initial raw sample and discarded sperm (cells not affected by the SSAW field and remained in the mainstream). Values are reported as mean ± s.d. for 3 independent experiments.

Sperm progressive motility, indicating sperm that are mostly swimming in straight lines or large circles, is one of the key parameters influencing the fertilization rate in assisted reproduction[60]. The progressive motility results in Fig. 3c demonstrate that the selected sperm population exhibit a considerably higher percentage of progressively motile sperm (83%) than both the initial raw sample (52%) and discarded subpopulation of sperm (36%). The applied SSAW field guides sperm with highly progressive motility out of the main flow stream to be retrieved from the selected cell outlet, while less motile cells and larger debris follow the main flow stream to be collected from the discarded cell outlet. These findings clearly indicate a process that selects for sperm with highly progressive motility in addition to size, as the applied acoustic force alone is not sufficient to push less motile and larger cells out of the main flow stream.

For control experiments in the absence of SAW actuation (see ESI† Fig. S1), the average concentration of sperm retrieved from the selected cell outlet was less than 0.6 M/ml (Fig. S1a) – only a quarter of the average concentration of selected cells under SAW actuation (Fig. 3a). Moreover, in the absence of an applied acoustic field, vitality and progressive

View Article Online
DOI: 10.1039/D0LC00457J

motility of selected sperm were comparable with the initial raw semen sample and the discarded subpopulation of sperm that remained in the mainstream (Fig. S1b,c), essentially rendering the selection process solely based on sperm motility insufficient to improve sperm quality. The results from the control experiments better highlight the key role of SAW actuation in the selection process achieved here.

Fig. 4 details the motility parameters for selected sperm and discarded cells as compared with the initial raw sample. The results indicate that the acoustofluidic device selected faster sperm with significantly higher values of VCL, VAP, and VSL as compared with the initial raw sample and discarded population. Specifically, selected sperm from the device exhibited 64%, 78% and 55% increase in VCL (from 31 μm/s to 51 μm/s), VAP (from 23 μm/s to 41 μm/s) and VSL (from 22 μm/s to 34 μm/s), respectively, compared to the initial raw sample ($P \leq 0.05$ in all cases), while immotile and relatively slow sperm were collected in the discarded sample (with VCL of 25 μm/s, VAP of 14 μm/s and VSL of 12 μm/s). Moreover, LIN, ALH and BCF were increased by 8.1% ($P=0.18$, not statistically significant), 32.3% ($P=0.22$, not statistically significant) and 11.1% ($P \leq 0.05$) for selected sperm as compared with the raw sample (See ESI† Table. S1). The results demonstrate that selected sperm swim straighter and faster by beating at larger flagellar wave amplitude and frequency (larger and faster oscillation of head). Selected sperm from controlled experiments, in the absence of an applied acoustic field, demonstrated a slight but insignificant increase in sperm motility parameters compared to the initial raw semen sample and the discarded subpopulation of sperm that remained in the mainstream (see ESI† Fig. S2). The results indicate that a separation strategy solely based on sperm motility is incapable of selecting sperm with considerably improved quality.

View Article Online
DOI: 10.1039/D0LC00457J

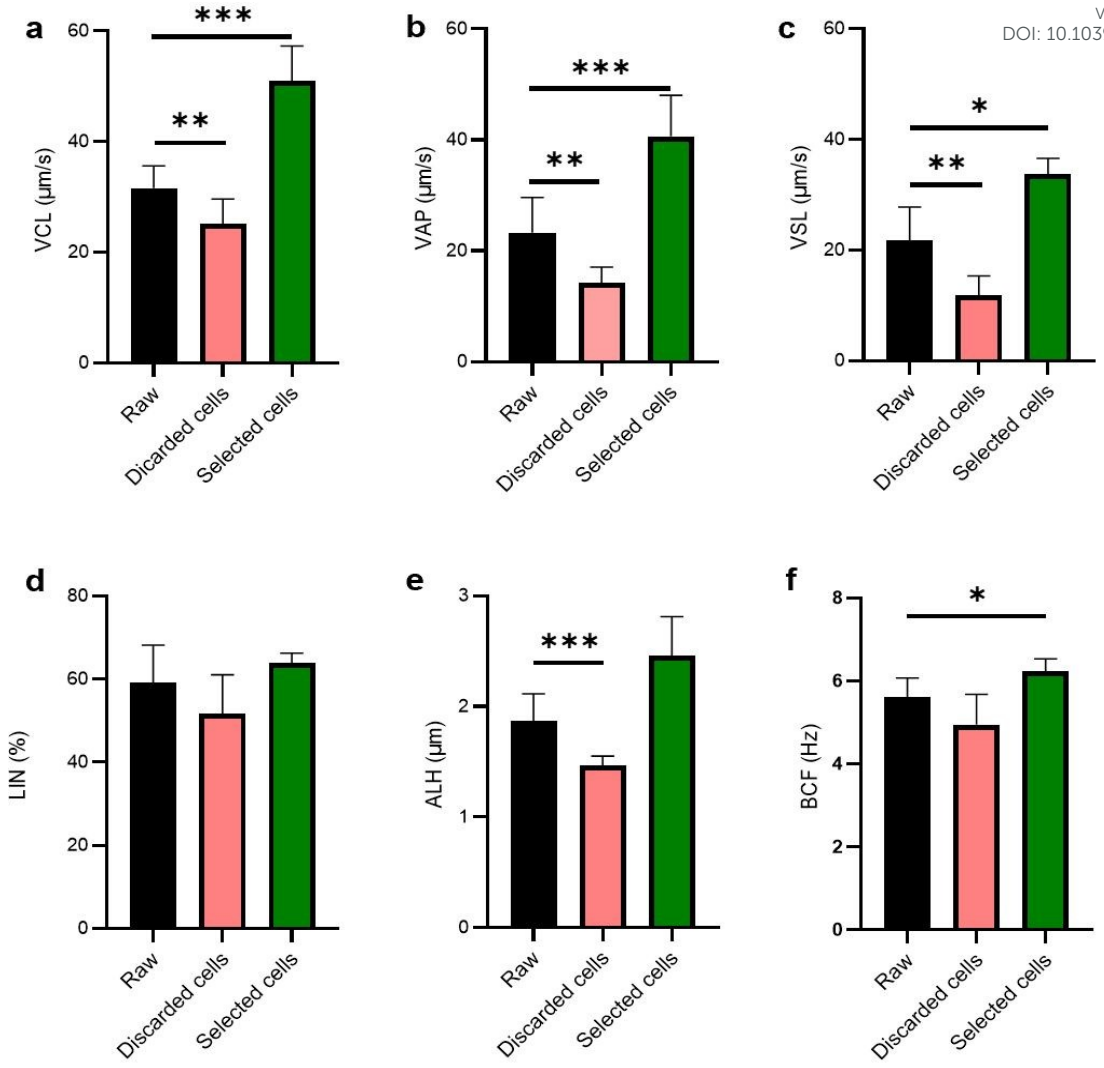

Figure 4. Sperm motility analysis. (a) Curvilinear velocity (VCL), (b) average path velocity (VAP), (c) straight line velocity (VSL), (d) linearity (LIN), (e) lateral head displacement (ALH), and (f) beat cross frequency (BCF) for selected sperm as compared with the raw sperm sample and discarded sperm. Values are reported as mean ± s.d. for 3 independent experiments where over 100 sperm where analysed in each experiment, *$P \leq 0.05$, **$P \leq 0.01$ and ***$P \leq 0.001$.

Sperm head morphology is an excellent marker of other sperm defects, including DNA damage due to non-orthodox DNA configurations[61], that significantly influence the choice of treatment in ART and subsequent embryo implantation and pregnancy rates[6263]. Bull sperm head morphology was assessed using haematoxylin-eosin staining, as shown in Fig. 5a-c. Despite a slight increase in head length and width (less than 1 µm), selected sperm demonstrated similar head morphology as compared with the initial raw sample and discarded cells, all within the range for morphologically normal sperm head (head length of 7-9 µm and width of 4-6 µm)[64]. Morphologically homogeneous quality of bull sperm in the initial raw sample mainly led to this comparable sperm head morphology characteristics, while the device was still capable of distinguishing small size differences between live and dead sperm (See ESI† Movie. S1). Due

to this similarity in size, sperm cells were subjected to similar drag and acoustic forces, thus allowing sperm motility to play the main role in the selection process.

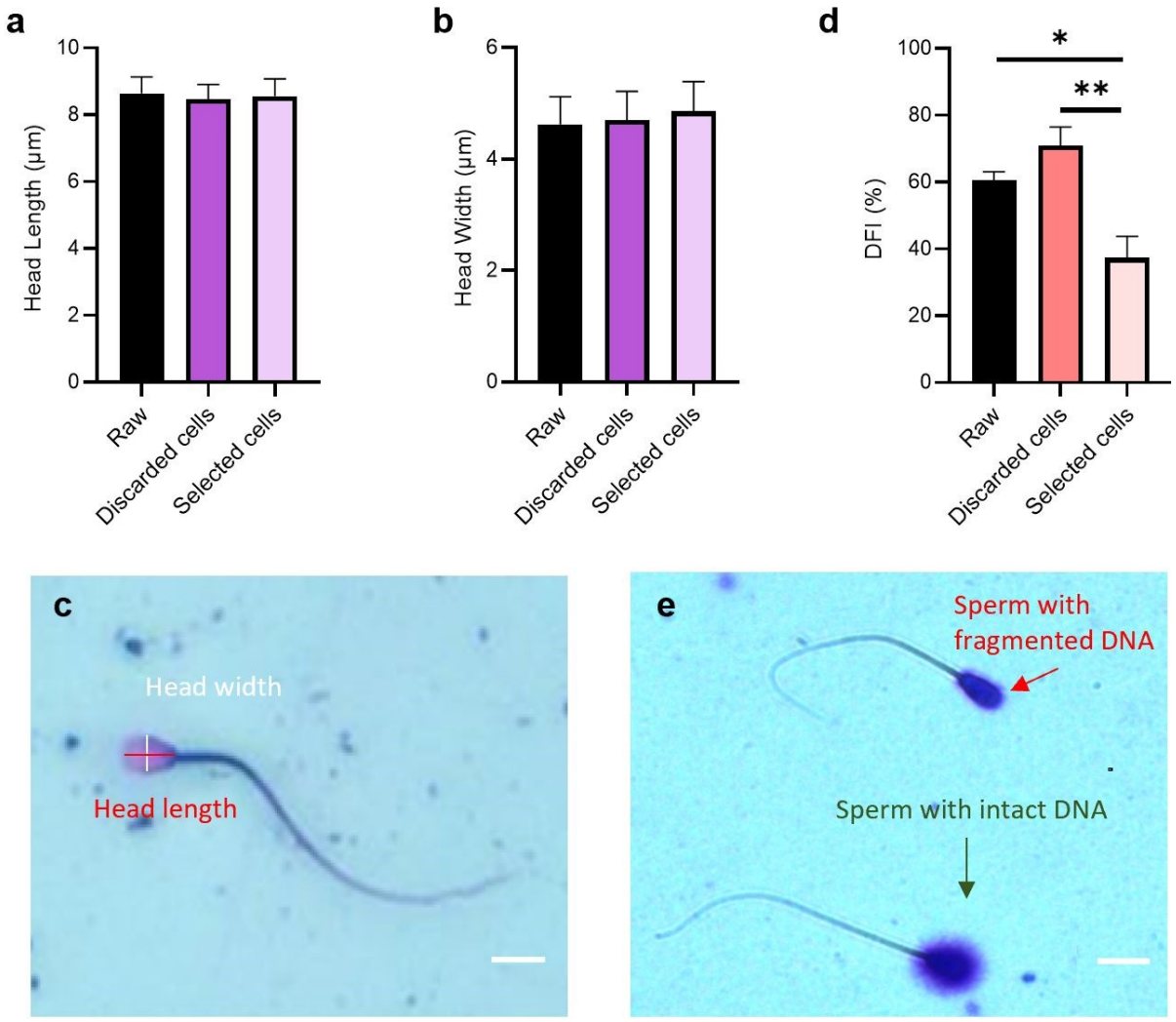

Figure 5. Sperm morphology and DNA integrity analysis. Sperm (a) head length and (b) head width for selected sperm as compared with the initial raw sample and discarded cells. (c) A representative image of sperm after staining with Haematoxylin and Eosin for morphological analysis. (d) DNA fragmentation index (DFI) of selected sperm and discarded cells in comparison with the raw sample. P values were determined using one-way ANOVA between B/A values from the SCD test, *P≤0.05, **P≤0.01. (e) A representative image of sperm with intact and damaged DNA from sperm chromatin dispersion test. Values are reported as mean ± s.d. for 3 independent experiments. Scale bars represent 10µm.

DNA integrity is an important indicator of sperm quality, significantly influencing the reproductive outcome and fertilization rate[2]. Sperm DNA damage is associated with low pregnancy rate, pregnancy loss in both IVF and ICSI, and de novo mutations in the offspring[65]. Sperm chromatin dispersion (SCD) test was used to assess DNA integrity (Fig. 5e), by quantifying the percentage of DNA fragmentation index (%DFI) as a measure of DNA strand breaks[59]. The %DFI results in Fig. 5d demonstrate a significant improvement in selected sperm DNA integrity compared to the initial raw sample. Specifically, the %DFI was 60.6 in the initial

View Article Online
DOI: 10.1039/D0LC00457J

raw sample and improved by 38 to 37.3 for selected sperm. By collecting sperm with intact DNA from the raw sample, the %DFI for discarded cells was 70.9 as expected. These finding indicate that the device select sperm with considerably higher DNA integrity.

Conclusions

We present an automated acoustofluidic approach for high-throughput isolation of sperm with normal head morphology and high DNA integrity from raw semen samples, processing ~140 sperm per second and selecting over 60,000 high-quality sperm in under 50 min. The device enables isolation of sperm from raw semen in a continuous-flow system by applying an acoustic field at 30° angle to the flow direction to laterally deflect sperm based on their size and motility. The device select sperm with over 50% and 60% improvement in vitality and progressive motility in 50 min, respectively, while providing clinically relevant volume and selected sperm number for the performance of IVF and ICSI (over 60,000 selected sperm in 30 μL). Selected sperm swim straighter and 64% faster by beating at larger flagellar wave amplitude and frequency, leading to improved fertilization rate in assisted reproduction. Moreover, sperm selected from the device show more than 38% improvement in DNA integrity. Taken together, our acoustofluidic sperm selection approach provides new opportunities to select sperm for assisted reproduction with the potential to improve fertilization outcome.

Acknowledgements

This work was supported by the Australian Research Council (ARC) Discovery Project Grant (DP190100343 to R.N.) and Monash Interdisciplinary Research Grants to R.N. and A.N. This work was performed in part at the Melbourne Centre for Nanofabrication (MCN) in the Victorian Node of the Australian National Fabrication Facility (ANFF).

References

1 J. Boivin, L. Bunting, J. a. Collins and K. G. Nygren, *Hum. Reprod.*, 2007, **22**, 1506–1512.
2 R. Nosrati, P. J. Graham, B. Zhang, J. Riordon, A. Lagunov, T. G. Hannam, C. Escobedo, K. Jarvi and D. Sinton, *Nat. Rev. Urol.*, 2017, **14**, 707–730.
3 N. E. Skakkebaek, E. Rajpert-De Meyts, G. M. Buck Louis, J. Toppari, A.-M. Andersson, M. L. Eisenberg, T. K. Jensen, N. Jorgensen, S. H. Swan, K. J. Sapra, S. Ziebe, L. Priskorn and A. Juul, *Physiol. Rev.*, 2015, **96**, 55–97.
4 R. M. Schultz, *Science (80-.).*, 2002, **296**, 2188–2190.
5 G. R. Dohle, *Int. J. Urol.*, 2010, **17**, 327–331.
6 L. M. Pastore, *Obstet. Gynecol.*, 2006, **107**, 953.
7 K. Shiraishi, H. Matsuyama and H. Takihara, *Int. J. Urol.*, 2012, **19**, 538–550.

8 M. Aboulghar, D. T. Baird, J. Collins, J. L. H. Evers, B. C. J. M. Fauser, C. B. Lambalk, E. Somigliana, A. Sunde, B. Tarlatzis, P. G. Crosignani, P. Devroey, E. Diczfalusy, K. Diedrich, L. Fraser, J. P. M. Geraedts, L. Gianaroli, A. Glasier and A. Van Steirteghem, *Hum. Reprod. Update*, 2009, **15**, 265–277.
9 A. Pinborg, *Hum. Reprod. Update*, 2005, **11**, 575–593.
10 R. Nosrati, M. Vollmer, L. Eamer, M. C. San Gabriel, K. Zeidan, A. Zini and D. Sinton, *Lab Chip*, 2014, **14**, 1142–1150.
11 L. Eamer, M. Vollmer, R. Nosrati, M. C. San Gabriel, K. Zeidan, A. Zini and D. Sinton, *Lab Chip*, 2016, **16**, 2418–2422.
12 R. K. Sharma and A. Agarwal, *Urology*, 1996, **48**, 835–850.
13 C. C. Approaches, *Male fertility book, Andrology*, .
14 R. R. Henkel and W. B. Schill, *Reprod. Biol. Endocrinol.*, 2003, **1**, 1–22.
15 G. M. Centola, R. Herko, E. Andolina and S. Weisensel, *Fertil. Steril.*, 1998, **70**, 1173–1175.
16 R. J. AITKEN and J. S. CLARKSON, *J. Androl.*, 1988, **9**, 367–376.
17 M. Szamatowicz, *Ginekol. Pol.*, 2016, **87**, 820–823.
18 R. Nosrati, A. Driouchi, C. M. Yip and D. Sinton, *Nat. Commun.*, 2015, **6**, 1–9.
19 E. K. Sackmann, A. L. Fulton and D. J. Beebe, *Nature*, 2014, **507**, 181–189.
20 S. M. Knowlton, M. Sadasivam and S. Tasoglu, *Trends Biotechnol.*, 2015, **33**, 221–229.
21 M. M. Gong, R. Nosrati, M. C. San Gabriel, A. Zini and D. Sinton, *J. Am. Chem. Soc.*, 2015, **137**, 13913–13919.
22 R. Nosrati, M. M. Gong, M. C. S. Gabriel, C. E. Pedraza, A. Zini and D. Sinton, *Clin. Chem.*, 2016, **62**, 458–465.
23 R. Nosrati, M. M. Gong, M. C. San Gabriel, A. Zini and D. Sinton, *Anal. Methods*, 2016, **8**, 6260–6264.
24 C. K. Tung, L. Hu, A. G. Fiore, F. Ardon, D. G. Hickman, R. O. Gilbert, S. S. Suarez and M. Wu, *Proc. Natl. Acad. Sci. U. S. A.*, 2015, **112**, 5431–5436.
25 C. K. Tung, F. Ardon, A. G. Fiore, S. S. Suarez and M. Wu, *Lab Chip*, 2014, **14**, 1348–1356.
26 M. Zaferani, S. H. Cheong and A. Abbaspourrad, *Proc. Natl. Acad. Sci. U. S. A.*, 2018, **115**, 8272–8277.
27 S. Tasoglu, H. Safaee, X. Zhang, J. L. Kingsley, P. N. Catalano, U. A. Gurkan, A. Nureddin, E. Kayaalp, R. M. Anchan, R. L. Maas, E. Tüzel and U. Demirci, *Small*, 2013, **9**, 3374–3384.
28 S. Wang, 2015, 1–3.
29 T. Chinnasamy, J. L. Kingsley, F. Inci, P. J. Turek, M. P. Rosen, B. Behr, E. Tüzel and U. Demirci, *Adv. Sci.*, , DOI:10.1002/advs.201700531.
30 J. Riordon, F. Tarlan, J. B. You, B. Zhang, P. J. Graham, T. Kong, Y. Wang, A. Lagunov, T. Hannam, K. Jarvi and D. Sinton, *Lab Chip*, 2019, **19**, 2161–2167.
31 B. S. Cho, T. G. Schuster, X. Zhu, D. Chang, G. D. Smith and S. Takayama, *Anal. Chem.*, 2003, **75**, 1671–1675.
32 T. M. El-Sherry, M. Elsayed, H. K. Abdelhafez and M. Abdelgawad, *Integr. Biol. (United Kingdom)*, 2014, **6**, 1111–1121.
33 L. Xie, R. Ma, C. Han, K. Su, Q. Zhang, T. Qiu, L. Wang, G. Huang, J. Qiao, J. Wang and J. Cheng, *Clin. Chem.*, 2010, **56**, 1270–1278.
34 B. De Wagenaar, S. Dekker, H. L. De Boer, J. G. Bomer, W. Olthuis, A. Van Den Berg and L. I. Segerink, *Lab Chip*, 2016, **16**, 1514–1522.
35 D. T. Chiu, A. J. deMello, D. Di Carlo, P. S. Doyle, C. Hansen, R. M. Maceiczyk and R. C. R. Wootton, *Chem*, 2017, **2**, 201–223.

36 A. T. Ohta, M. Garcia, J. K. Valley, L. Banie, H. Y. Hsu, A. Jamshidi, S. L. Neale, T. Lue and M. C. Wu, *Lab Chip*, 2010, **10**, 3213–3217.
37 B. Landenberger, H. Höfemann, S. Wadle and A. Rohrbach, *Lab Chip*, 2012, **12**, 3177–3183.
38 M. P. MacDonald, G. C. Spalding and K. Dholakia, *Nature*, 2003, **426**, 421–424.
39 Y. Wang, Y. Zhao and S. K. Cho, *J. Micromechanics Microengineering*, 2007, **17**, 2148–2156.
40 V. Magdanz, S. Sanchez and O. G. Schmidt, *Adv. Mater.*, 2013, **25**, 6581–6588.
41 N. Xia, T. P. Hunt, B. T. Mayers, E. Alsberg, G. M. Whitesides, R. M. Westervelt and D. E. Ingber, *Biomed. Microdevices*, 2006, **8**, 299–308.
42 P. R. C. Gascoyne and J. Vykoukal, *Electrophoresis*, 2002, **23**, 1973–1983.
43 A. Haake, A. Neild, D. H. Kim, J. E. Ihm, Y. Sun, J. Dual and B. K. Ju, *Ultrasound Med. Biol.*, 2005, **31**, 857–864.
44 C. Devendran, J. Carthew, J. E. Frith and A. Neild, *Adv. Sci.*, , DOI:10.1002/advs.201902326.
45 A. Neild, S. Oberti and J. Dual, *Sensors Actuators, B Chem.*, 2007, **121**, 452–461.
46 M. Hill, Y. Shen and J. J. Hawkes, *Ultrasonics*, 2002, **40**, 385–392.
47 S. C. S. Lin, X. Mao and T. J. Huang, *Lab Chip*, 2012, **12**, 2766–2770.
48 G. Destgeer, K. H. Lee, J. H. Jung, A. Alazzam and H. J. Sung, *Lab Chip*, 2013, **13**, 4210–4216.
49 I. Leibacher, P. Reichert and J. Dual, *Lab Chip*, 2015, **15**, 2896–2905.
50 K. Xu, C. P. Clark, B. L. Poe, J. A. Lounsbury, J. Nilsson, T. Laurell and J. P. Landers, *Anal. Chem.*, 2019, **91**, 2186–2191.
51 X. Ding, P. Li, S. C. S. Lin, Z. S. Stratton, N. Nama, F. Guo, D. Slotcavage, X. Mao, J. Shi, F. Costanzo and T. J. Huang, *Lab Chip*, 2013, **13**, 3626–3649.
52 R. Habibi and A. Neild, *Lab Chip*, 2019, **19**, 3032–3044.
53 C. Devendran, T. Albrecht, J. Brenker, T. Alan and A. Neild, *Lab Chip*, 2016, **16**, 3756–3766.
54 A. Fakhfouri, C. Devendran, D. J. Collins, Y. Ai and A. Neild, *Lab Chip*, 2016, **16**, 3515–3523.
55 D. J. Collins, T. Alan and A. Neild, *Lab Chip*, 2014, **14**, 1595–1603.
56 H. Jiang, J. woo Kwon, S. Lee, Y. J. Jo, S. Namgoong, X. rui Yao, B. Yuan, J. bao Zhang, Y. K. Park and N. H. Kim, *Sci. Rep.*, 2019, **9**, 1–12.
57 J. P. Leão-Neto, J. H. Lopes and G. T. Silva, *J. Acoust. Soc. Am.*, 2020, **147**, 2177–2183.
58 L. Eamer, R. Nosrati, M. Vollmer, A. Zini and D. Sinton, *Biomicrofluidics*, , DOI:10.1063/1.4928129.
59 C. M. Feijó and S. C. Esteves, *Fertil. Steril.*, , DOI:10.1016/j.fertnstert.2013.09.002.
60 L. Simon and S. E. M. Lewis, *Syst. Biol. Reprod. Med.*, 2011, **57**, 133–138.
61 M. Enciso, H. Cisale, S. D. Johnston, J. Sarasa, J. L. Fernández and J. Gosálvez, *Theriogenology*, 2011, **76**, 23–32.
62 E. Aksoy, T. M. Aktan, S. Duman and G. Cuce, *Int. J. Morphol.*, 2012, **30**, 1544–1550.
63 I. Taşdemir, M. Taşdemir, Ş. Tavukçuoğlu, S. Kahraman and K. Biberoğlu, *Hum. Reprod.*, 1997, **12**, 1214–1217.
64 M. E. Beletti, L. D. F. Costa and M. P. Viana, *Anim. Reprod. Sci.*, 2005, **85**, 105–116.
65 A. Zini and M. Sigman, *J. Androl.*, 2009, **30**, 219–229.